JOINT INSTITUTE FOR NUCLEAR RESEARCH

Dzhelepov laboratory of Nuclear Problems

FINAL REPORT ON THE START PROGRAMME

Fast Monte Carlo simulation of the JUNO detector response based on slow Monte Carlo simulation

Supervisor:

Dr. Oleg Yurievich Smirnov

Student:

Elizaveta Korzheva, Russia

Peter the Great St.Petersburg

Polytechnic University

Participation period:

February 18 – April 4,

Winter Session 2026

Dubna, 2026

1. Introduction

1.1 JUNO detector

JUNO (Jiangmen Underground Neutrino Observatory) is a large liquid scintillator detector located in an underground laboratory at a depth of 700 meters in Guangdong Province, southern China. The primary physics goal of the detector is to determine the neutrino mass hierarchy.

The heart of the detector is a spherical acrylic vessel with an inner diameter of 35.4 meters, filled with 20 kilotons of LAB-based (linear alkylbenzene) liquid scintillator (see Figure 1.1):

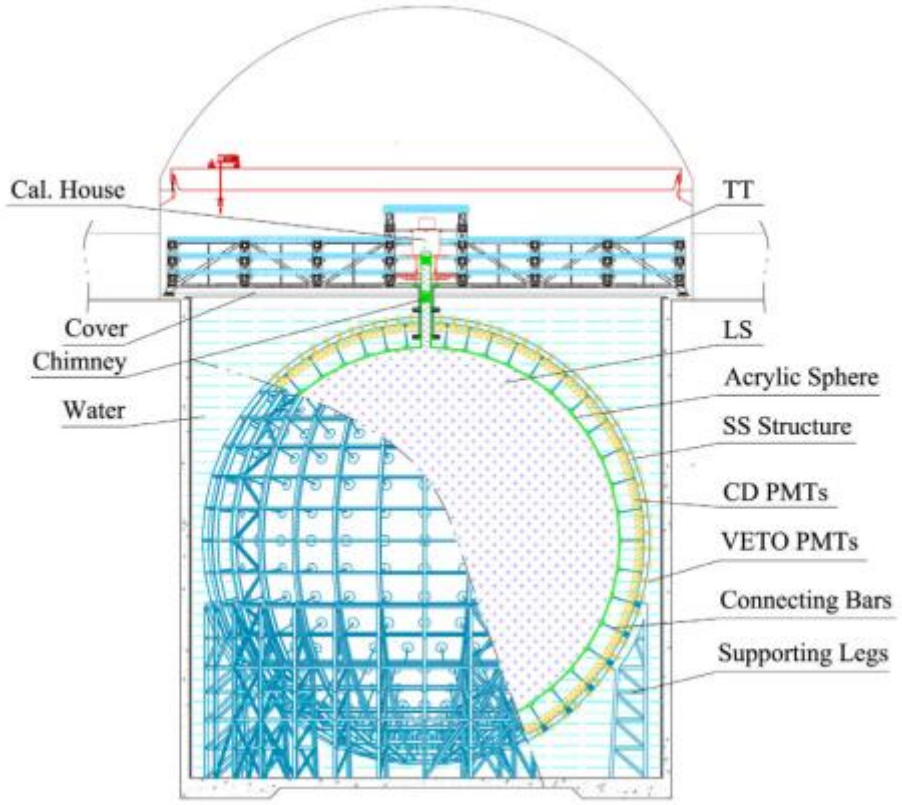

Fig. 1.1 - Schematic diagram of the JUNO detector

Around this sphere is one of the densest photomultiplier tube (PMT) systems ever built: approximately 18,000 large 20-inch PMTs and 25,000 small 3-inch PMTs. Together, they cover about 75% of the inner surface of the detector, allowing for the maximum possible number of photons to be collected.

The central detector is located inside a large cylindrical pool filled with 35 kilotons of ultrapure water. Water serves as a shield against natural radioactivity and functions as a Cherenkov veto detector for cosmic-ray muons: 2400 PMTs installed in the water pool detect Cherenkov radiation, allowing background events to be identified and rejected. Additionally, above the main detector, there is a Top Tracker made of plastic scintillator strips, which provides more precise measurement of muon tracks.

The main signal detected in the JUNO detector is from reactor antineutrinos produced at the Yangjiang and Taishan nuclear power plants (with a total thermal power of 26.6 GW), located at an equal distance of ~53 km from the detector. Antineutrinos are detected via inverse beta decay events:

$$\widetilde{\nu_e} + p \rightarrow e^+ + n$$

The positron annihilates quickly, producing a prompt signal, while the neutron is captured by a proton after ~200 μs, forming a delayed signal. The expected detection rate for such events is about 60 per day.

To determine the neutrino mass hierarchy, the JUNO detector must achieve an energy resolution of 3%/√E(MeV). According to the latest data, the actual resolution of JUNO is about 3% at 1 MeV, with variations ranging from ≈2.9% in the center to ≈3.4% at the periphery, as confirmed by calibration and measurements of reactor and solar neutrinos. This imposes stringent requirements on the accuracy of energy reconstruction and the modeling of light propagation. Thus, JUNO represents a complex optical system in which the generation, propagation, and detection of light play a key role.

1.2 The problem of computational expensiveness of full-scale simulation

The standard (slow) simulation of the JUNO detector response is based on the Geant4 package and involves detailed tracking of each scintillation photon. In this approach, millions of photons are generated for each event, each of which

propagates through the detector considering absorption, Rayleigh scattering, and re-emission.

Such an approach provides high accuracy but comes with an extremely high computational cost. For a detector of JUNO's scale, a single event can generate tens of millions of photons, and large-scale Monte Carlo calculations require millions of CPU hours. As a result, the use of full simulation becomes practically impossible for tasks that require large statistics, such as optimizing reconstruction algorithms or evaluating systematic uncertainties.

At the same time, full simulation is not always necessary. In many tasks, it is sufficient to correctly reproduce the main characteristics of the detector response without detailed tracking of each photon. Therefore, the development of simplified and computationally efficient simulation methods becomes relevant. This approach is based on empirical light collection maps derived from calibration data. This work is aimed at the development and study of such an approach.

1.3 The idea of fast simulation

An alternative to full simulation is the empirical approach, in which detailed photon tracking is replaced by an effective description of the detector response. Such methods were previously used in the CTF and Borexino experiments, where light collection maps obtained from calibration data were employed.

The main idea is to replace the tracking of individual photons with a precomputed response function - a PMT light collection map. In a spherical detector such as JUNO, the PMT signal is primarily determined by the distance to the event and the relative angle. The light collection map incorporates complex optical processes (scattering, absorption, reflection) and can be obtained either from full simulation or from real data.

Once the map is constructed, event simulation becomes significantly simplified: the expected number of photoelectrons at each PMT is determined from

the event position, after which statistical fluctuations are considered. This reduces the generation time for a single event from seconds to milliseconds.

The model implemented in this work is simplified (in particular, it does not include simulation of the time structure of signals), but it allows the main characteristics of the detector response in the central region to be reproduced.

2. PMT light collection function (map)

2.1 Location and types of photomultiplier tubes in the central detector

In this work, only the large (20-inch) photomultiplier tubes (PMTs) of the JUNO central detector are considered. For simulation and data analysis, the coordinates of all PMTs are used, defined in a reference frame with its origin at the center of the detector.

The light detection system of the central detector includes several types of large PMTs. The main ones are microchannel plate photomultiplier tubes (MCP PMTs), manufactured by Northern Night Vision Technology Co., and dynode photomultiplier tubes, manufactured by Hamamatsu Photonics.

The microchannel PMTs are divided into two subtypes: NNVT (2720 PMTs) and HighQE NNVT (9825 PMTs), while the number of dynode PMTs is 4997. However, within the framework of this approach, both subtypes of microchannel photomultipliers are combined into a single group, since their characteristics are not distinguished in the model used. Thus, two types of PMTs are considered hereafter: microchannel and dynode.

In the JUNO software, each photomultiplier tube is assigned a unique identifier ranging from 0 to 17611, along with its spatial coordinates (see Figure 1.2). All PMTs are located on a sphere of radius $L_0 \approx 19.4$ m, the center of which coincides with the center of the detector.

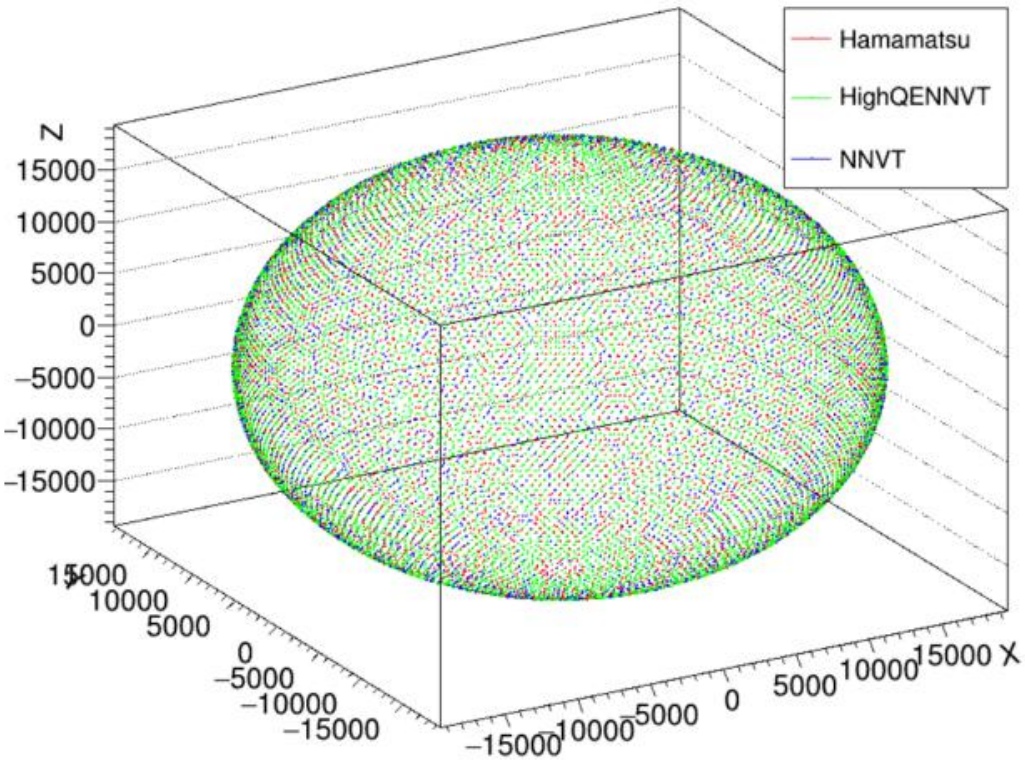

Fig. 1.2 - Arrangement of the PMTs in the central detector, separated by type: Hamamatsu (red), HighQE NNVT (green), and NNVT (blue). Coordinates are given in mm.

The PMT coordinates correspond to the geometric center of the photocathode surface. This was determined by simulating events at the center of the detector, in which the impact points of scintillation photons on the photocathode were analyzed. However, for simulation purposes, it is more appropriate to use the coordinates of the outer point of the photocathode surface (its "apex").

The transition from the coordinates of the photocathode center to its surface is performed using a characteristic offset, which is approximately 190 mm for dynode PMTs and about 184 mm for microchannel PMTs. This offset is considered when constructing the geometry of the model.

Thus, the precise specification of the coordinates and types of photomultiplier tubes is a necessary element for the correct description of the detector geometry and the subsequent construction of the light collection function.

2.2 Detector geometry

The position of each event can be described by coordinates $\mathrm{r} = \{x, y, z\}$ in the reference frame associated with the center of the detector.

In the coordinate system associated with the i-th PMT, the event position is characterized by two parameters:

- the distance L_i from the PMT to the event point;
- the polar angle θ_i' at which the PMT "sees" the event (the angle is measured from the PMT axis passing through the center of the detector).

Axial symmetry of the photocathode sensitivity is assumed, therefore the azimuthal angle in the PMT reference frame is not required.

Another pair of coordinates can be introduced to describe the event position:

- The distance from the center of the detector to the event

$r = \sqrt{x^2 + y^2 + z^2}$ (this coordinate is the same for all PMTs);

- The angle θ_i between the position vector of the event r and the position vector of the i-th PMT, R_i.

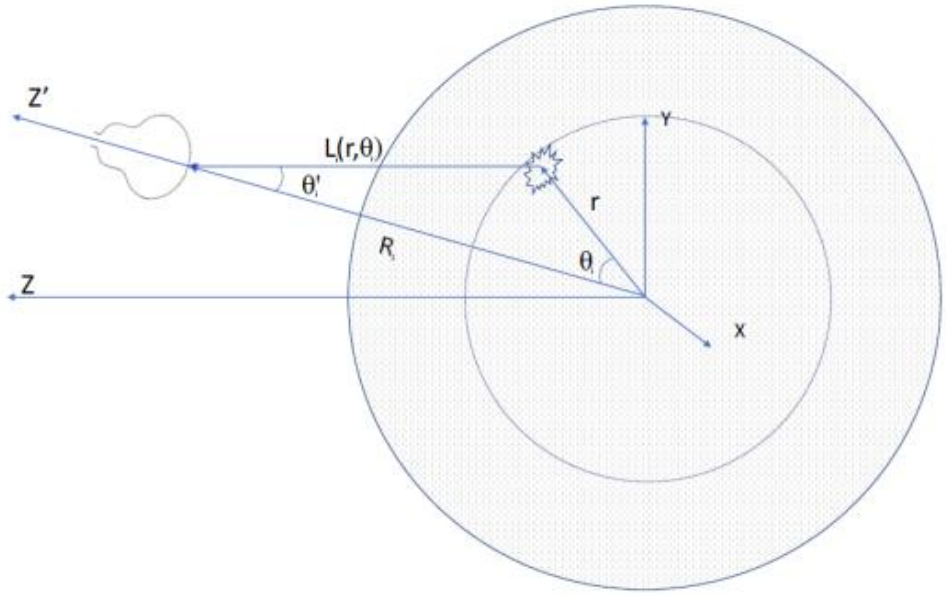

Fig. 2.1 - Positions of the PMTs and the event, along with the coordinates used to describe them: $\{r, \cos\theta_i\}$ and $\{L_i, \cos\theta_i'\}$. The shaded volume represents the central detector filled with scintillator: a sphere of radius R = 17.7 m

All transformations between these coordinate systems can be easily obtained from the geometry:

$$\cos\ \theta_i = \frac{\mathrm{R}_i \cdot \mathrm{r}}{R_i r}$$

$$L_i(r, \cos\ \theta_i) = \sqrt{r^2 + R_i^2 - 2rR_i \cos\ \theta_i}$$

$$\cos\ \theta_i'(r, \cos\ \theta_i) = \frac{R_i - r\cos\ \theta_i}{L_i(r, \theta_i)}$$

Knowing the coordinates of all PMTs in the detector, for each event the coordinates can be calculated both in the $\{r, \cos\ \theta_i\}$ system and in the $\{L_i, \cos\ \theta_i'\}$ system. This is necessary for the subsequent calculation of the PMT light collection map.

2.3 Light collection function

A key concept in fast simulation is the PMT light collection function (map) $f_{\text{pm}}(r, \cos\ \theta)$. It describes how the average charge collected by a given PMT varies depending on the position of the event relative to that PMT.

Let us first define the average charge collected by a single PMT for an event at the center of the detector. If the total average charge collected by all PMTs at the center of the detector is $\langle Q_0 \rangle$, then the average per PMT is:

$$\mu_0 = \frac{\langle Q_0 \rangle}{N_{\text{PMT}}} p.e.$$

However, the PMTs in the detector have different sensitivities. To account for this, a relative sensitivity s_i is introduced for each PMT:

$$s_i = \frac{\mu_i}{\mu_0}$$

where μ_i is the average charge recorded by the i-th PMT for events at the center of the detector.

Now consider an event at an arbitrary point in the detector. The average charge collected by the i-th PMT in this event can be written as:

$$\mu_i(r, \cos\ \theta_i) = \mu_0 \cdot s_i \cdot f_{\text{pm}}(r, \cos\ \theta_i)$$

Here $f_{\text{pm}}(r, \cos\ \theta_i)$ is the desired PMT light collection function. It shows how many times the average collected charge changes when the event is shifted from the center to a point with coordinates $\{r, \cos\ \theta_i\}$ relative to the given PMT. By definition, at the center of the detector, $f_{pm}(0, \cos\ \theta_i) = 1$ for any $\cos\theta_i$.

The total average charge collected by all PMTs for an event at point r is:

$$Q(\mathbf{r}) = \sum_{i=1}^{N_{\text{PMT}}} \mu_0\, s_i f_{\text{pm}}(r, \cos\ \theta_i)$$

Thus, if μ_0, the relative sensitivities s_i, and the light collection function f_{pm} are known, then for any event position the expected response of each PMT can be calculated without simulating the propagation of individual photons.

To describe the dependence of the PMT response on the event position, the PMT light collection function (map) $f_{\text{PMT}}(r, \cos\,\theta)$ is used. It shows how many times the average collected charge changes when the event is shifted from the center of the detector to a point with coordinates $\{r, \cos\,\theta_i\}$ relative to the given PMT.

For the analytical description of the light collection map, the following approximation is used:

$$f_{\text{PMT}}(r, \cos\theta) = f_0 \cdot \left(\frac{L_0}{L(r, \cos\theta)}\right)^m \cdot cos^n\theta'(r, \cos\theta) \cdot$$

$$\cdot \exp\left(-\frac{L(r, cos\theta) - L_0}{L_{att}}\right) + D$$

where:

- r and $\cos\theta$ are the coordinates of the event relative to the PMT;
- $L(r, \cos\,\theta)$ - is the distance from the event to the PMT;
- $\theta'(r, \cos\,\theta)$ - is the angle between the direction to the event and the PMT axis;
- $L_0 = 19.4$ m - is the distance from the center of the detector to the PMT;
- f_0 - is a normalization factor (≈ 1);
- m - is a parameter fixed at $m = 2$ (isotropic light propagation);
- n - a parameter describing the angular dependence of the PMT sensitivity;

- L_{att} - is the effective light absorption length in the scintillator (on the order of ≈ 20 m);
- D - is a constant accounting for the contribution of the PMT dark count.

With $D = 0$ and $f_0 = 1$, the PMT light collection function equals 1 at the center of the detector.

The light collection function allows the average expected charge μ_i to be calculated for each PMT, after which the number of photoelectrons is drawn from a Poisson distribution, and the charge of each photoelectron is drawn from the single-electron spectrum of the corresponding PMT. This forms the basis of the fast simulation algorithm.

3. Fast simulation of the detector response

3.1 Basic principles of simulation

Fast simulation is based on replacing full optical photon tracking with a precomputed response function - the PMT light collection map. Instead of simulating the propagation of millions of photons through the detector, the average expected number of photoelectrons μ_i is directly calculated for each PMT based on the event position, after which statistical fluctuations are sampled.

The fast event simulation algorithm implemented in this work is quite simple. It uses the previously introduced concepts and parameters to determine which PMTs will register the scintillation flash and how much charge will be collected by each of them. The parameters of the single-electron spectrum of the large PMTs in the JUNO detector are also of great importance.

3.2 Energy estimators

In scintillation experiments with a large number of PMTs, a detected event is primarily a set of charges recorded by each PMT $\{q_i\}$. To reconstruct the event energy, energy estimators are used - observable quantities that depend on the energy.

In this work, two simplest energy estimators are considered:

1. Total collected charge Q - the sum of charges over all PMTs of the detector:

$$Q = \sum_{i}^{N_{\text{PMT}}} q_i,$$

where q_i is the charge in photoelectrons (p.e.) recorded by the i-th PMT.

2. The number of fired PMTs N_{pm} - the number of PMTs that recorded at least one photoelectron after passing the discriminator threshold:

$$N_{\text{pm}} = \sum_{i}^{N_{\text{PMT}}} \Theta(\, q_i - q_{\text{th}_i}),$$

where $\Theta(x)$ is the Heaviside step function, and q_{th_i} is the discriminator threshold for the i-th PMT.

These quantities allow the event energy and the energy resolution of the detector to be estimated.

The obtained light collection map makes it possible to construct reconstructed energy estimators corrected for the event coordinates.

For the charge variable, the reconstructed estimator has the form:

$$Q_{\text{Rec}} = f_{\text{eq}} \frac{Q(x, y, z)}{f_{\text{Det}}(\vec{r})},$$

where $f_{\text{Det}}(\vec{r})$ is the light collection function of the detector:

$$f_{\text{Det}}(\vec{r}) = \frac{1}{N_{\text{equiv}}} \sum_{i} s_i \, f_{\text{pm}}(r, \theta_i(\vec{r})).$$

here $N_{\text{equiv}} = \sum_i s_i$ is the sum of the relative sensitivities of all operational PMTs (normalization coefficient).

For the number of fired PMTs, the reconstructed estimator taking into account the discriminator threshold is written as:

$$N_{\text{Rec}} = f_{\text{nc}}^{\text{pt}}(\mu_0, \vec{r}) \cdot N_{\text{eq}}(\vec{r})$$

where

- $N_{\text{eq}}(\vec{r}) = f_{\text{eq}} \cdot N_{\text{pm}}(\vec{r})$ - is the normalized number of fired PMTs;

  $f_{\text{eq}} = N_{\text{PMT}}(0)/N_{\text{PMT}}(t)$ - is the equalization factor, N(t) - the number of operational PMTs at time t.

- the correction factor $f_{\text{nc}}^{\text{pt}}$ accounts for the difference between the probability

of the PMT firing at the center of the detector and at the reconstructed point:

$$f_{\mathrm{nc}}^{\mathrm{pt}}(\mu_0, \vec{r}) \approx \frac{\sum(1 - e^{-s_i\mu_0}(1 + p_t s_i \mu_0))}{\sum(1 - e^{-s_i\mu_0 f_{\mathrm{pm}}(r,\theta_i(\vec{r}))}(1 + p_t s_i \mu_0 f_{\mathrm{pm}}(r, \theta_i(\vec{r}))))},$$

where p_t is the fraction of the single-electron spectrum below the discriminator threshold.

The mean values of the corrected variables correspond to the mean values for a source of the same energy placed at the center of the detector. Thus, the part related to the variation of the average detector response over the volume is excluded from the expressions for the energy resolution.

3.3 Fast simulation algorithm

The fast simulation algorithm implemented in this work includes the following steps:

- Drawing of event coordinates. Depending on the user's choice, the event coordinates $\vec{r} = \{x, y, z\}$ are either fixed at the center of the detector ($r = 0$) or drawn from a uniform distribution within a sphere of radius $R = 10$ m.
- Loop over PMT types (Hamamatsu and NNVT):

  For every type, the parameters of the μ_0 distribution (a Gaussian distribution with mean μ_0 and width σ_{μ_0}, depending on the PMT type) and the parameters of the light collection map f_{pm} are set.

- Loop over all PMTs (j = 1…17612):
  - The type of the j-th PMT is determined. If the PMT type does not match the current one, proceed to the next PMT.
  - Correction of PMT coordinates: shift from the photocathode center to its apex with a factor of 0.9902 for Hamamatsu PMTs and 0.9905 for NNVT PMTs.
  - Geometry calculation:

$$L_j = \sqrt{(x_i - x_{\text{pm}})^2 + (y_i - y_{\text{pm}})^2 + (z_i - z_{\text{pm}})^2},$$

$$\cos\theta_j = \frac{r_i^2 + (L_0 \cdot R_{\text{corr}})^2 - L_j^2}{2 r_i L_0 R_{\text{corr}}},$$

where $L_0 = 19434$ mm is the distance from the center of the detector to the PMT, and R_{corr} is the PMT coordinate correction factor (depends on the PMT type).

- Drawing a random value of μ_0 from a Gaussian distribution with parameters specified for the given PMT type.
- Determination of the relative sensitivity $\boldsymbol{s_i}$ for the given PMT. If the simulation accounts for the spread in PMT sensitivities, then $\boldsymbol{s_i}$ is taken from precomputed calibration values for each PMT; otherwise, it is set to $\boldsymbol{s_i} = 1$.
- Calculation of the average expected number of photoelectrons:

$$\mu_i = \mu_0 \cdot s_i \cdot f_{\text{pm}}(r_i, \cos\ \theta_j).$$

- Drawing the number of photoelectrons N_{PE} from a Poisson distribution with mean μ_i.

- Loop over each photoelectron (from 1 to N_{PE}):
  - Drawing of the charge dQ from the single-electron spectrum of this PMT;
  - Accumulation of charge Q_{pmt} for the given PMT.
  - Addition of Q_{pmt} to the total event charge Q and to the charge accumulated by the PMTs of this type.
  - Increment of the counter of fired PMTs N and the counter of fired PMTs of this type by 1.
- Filling of histograms after completing the loops over all PMTs.
- Calculation of the reconstructed quantities.

For each event (with random coordinates), the following additional calculations are performed:

- Восстановление координат события с гауссовой погрешностью ($\sigma = 100$ мм):
- Reconstruction of the event coordinates with a Gaussian error ($\sigma = 100$ mm):

$$x_{\text{rec}} = x_i + \mathcal{N}(0, \sigma_{\text{rec}}), y_{\text{rec}} = y_i + \mathcal{N}(0, \sigma_{\text{rec}}), z_{\text{rec}} = z_i + \mathcal{N}(0, \sigma_{\text{rec}}).$$

- Calculation of the detector light collection function at the reconstructed point for each PMT type:

$$f_{\text{Det}}^{(t)} = \frac{1}{N_{\text{PMT}}^{(t)}} \sum_{i \in \text{тип } t} s_i \cdot f_{\text{pm}}(r_{\text{rec}}, \cos\,\theta_i),$$

where $N_{\text{PMT}}^{(t)}$ - the number of PMTs of this type, s_i is the relative sensitivity of the i-th PMT.

- Calculation of the reconstructed total charge (corrected for position):

$$Q_{0,\text{rec}} = \frac{Q_{\text{Ham}}}{f_{\text{Det}}^{(\text{Ham})}} + \frac{Q_{\text{NNVT}}}{f_{\text{Det}}^{(\text{NNVT})}}$$

where Q_{Ham} and Q_{NNVT} - the charges collected by the PMTs of the corresponding types.

- Calculation of correction factors for the number of fired PMTs (considering the threshold $p_t = 0.1$):

$$f_{\text{nc}}^{pt(t)} = \frac{\sum_i \left(1 - e^{-s_i \mu_0^{(t)}} (1 + p_t s_i \mu_0^{(t)})\right)}{\sum_i \left(1 - e^{-s_i \mu_0^{(t)} f_{\text{pm}}(r_{\text{rec}}, \cos\,\theta_i)}\right)\left(1 + p_t s_i \mu_0^{(t)} f_{\text{pm}}(r_{\text{rec}}, \cos\,\theta_i)\right)},$$

where $\mu_0^{(t)}$ - the average charge per PMT of this type for an event at the center of the detector.

- Calculation of the reconstructed number of fired PMTs:

$$N_{0,\mathrm{rec}} = f_{\mathrm{nc}}^{pt(\mathrm{Ham})} \cdot N_{\mathrm{Ham}} + f_{\mathrm{nc}}^{pt(\mathrm{NNVT})} \cdot N_{\mathrm{NNVT}},$$

where N_{Ham} and N_{NNVT} - the number of fired PMTs of the corresponding types.

- Calculation of true (reference) values for comparison:

$$Q_{0,\mathrm{true}} = \mu_0^{(\mathrm{Ham})} \cdot N_{\mathrm{PMT}}^{(\mathrm{Ham})} + \mu_0^{(\mathrm{NNVT})} \cdot N_{\mathrm{PMT}}^{(\mathrm{NNVT})},$$
$$N_{0,\mathrm{true}} = N_{\mathrm{PMT}}^{(\mathrm{Ham})} \cdot \left(1 - e^{-\mu_0^{(\mathrm{Ham})}}\right) + N_{\mathrm{PMT}}^{(\mathrm{NNVT})} \cdot \left(1 - e^{-\mu_0^{(\mathrm{NNVT})}}\right)$$

where $\mu_0^{(\mathrm{Ham})}$ and $\mu_0^{(\mathrm{NNVT})}$ - the average charge per PMT for events at the center of the detector for Hamamatsu and NNVT PMTs. $N_{\mathrm{PMT}}^{(\mathrm{Ham})} = 4997$ and $N_{\mathrm{PMT}}^{(\mathrm{NNVT})} = 12615$ - are the numbers of PMTs of each type.

3.4 Parameters and input data used

The following input data, obtained from the slow simulation, are used for the operation of the algorithm:

- Coordinates and types of PMTs;
- The parameter μ_0 - the average charge collected by a single PMT for an event at the center of the detector (determined separately for each PMT type from the slow simulation).
- Relative sensitivities s_i;
- PMT light collection map $f_{\mathrm{pm}}(r, \cos\,\theta)$;
- Single-electron spectra (SPE spectra).

3.5 Generation of observable quantities

As a result of the algorithm, histograms of two main observable quantities are generated for each event:

- Total collected charge Q (in photoelectrons);

- Number of fired PMTs N_{pm}.

These histograms, constructed from a large number of generated events, allow the energy resolution of the detector to be estimated and the results of the fast simulation to be compared with those of the slow simulation.

4. Results for events at the center of the detector

4.1. Slow simulation (Po-210 at the center)

To obtain the parameters for the fast simulation, a slow simulation of the α-decay of polonium-210 ^{210}Po at the center of the JUNO detector was performed. The total collected charge, averaged over all PMTs, allows the average charge per PMT at the center of the detector to be determined:

$$\mu_0 = \frac{\langle Q_0 \rangle}{N_{\text{PMT}}}$$

As a result of processing the slow simulation, the following μ_0 values were obtained for the two types of PMTs:

Type of PMTs	$\mu_0(p.e.)$
Hamamatsu (HPK)	0.0452729
NNVT (MCP)	0.0490395

These values were used as input parameters for the fast simulation.

4.2. Fast simulation at the center of the detector

The fast event generator was run with fixed event coordinates ($r = 0$) and the μ_0 parameters obtained from the slow simulation. For each event, the values of the total charge collected by the PMTs of each type were generated. A total of 10^5 events were generated.

4.3. Comparison of distributions

For quantitative comparison of the fast and slow simulations, a script was developed that constructs histograms of the difference (fast - slow) and the ratio (fast / slow), and calculates χ^2 using the formula:

$$\chi^2 = \sum_i \frac{(N_{\text{slow},i} - N_{\text{fast},i})^2}{N_{\text{slow},i} + N_{\text{fast},i}},$$

where the summation is performed only over bins with a statistic of at least 20 events.

The comparison results are presented in the table:

Type of PMTs	χ^2	ndf	χ^2/ndf
Hamamatsu (HPK)	162.1	100	1.62
NNVT (MCP)	468.5	184	2.55

Figures 4.1–4.4 show the histograms of charges and the number of fired PMTs obtained from the fast and slow simulations. Figure 4.5 shows a comparison of the fast and slow simulations.

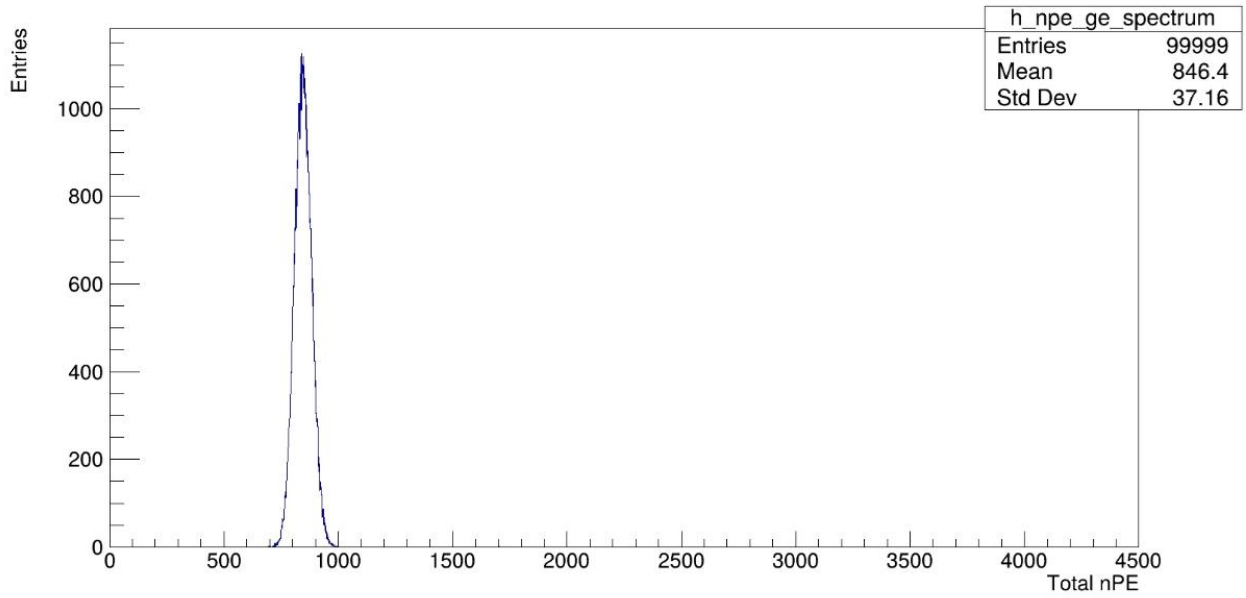

Figure 4.1 - Distribution of the total charge collected by PMTs of both types (Hamamatsu and NNVT) obtained from the slow simulation

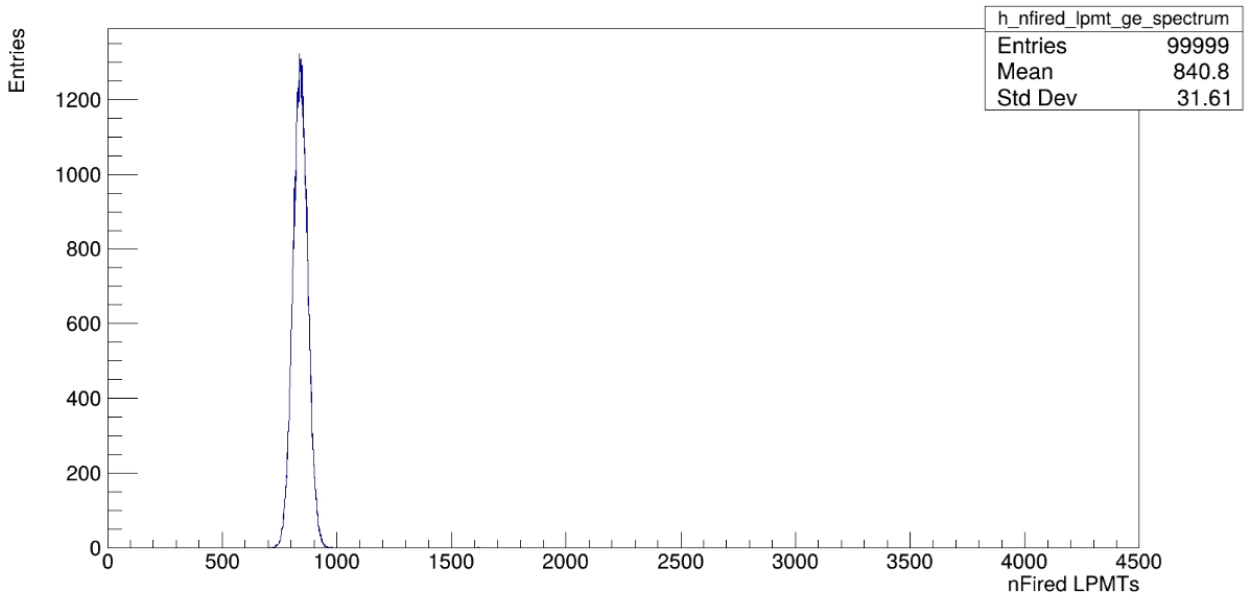

Figure 4.2 - Distribution of the number of fired PMTs of both types (Hamamatsu and NNVT) obtained from the slow simulation

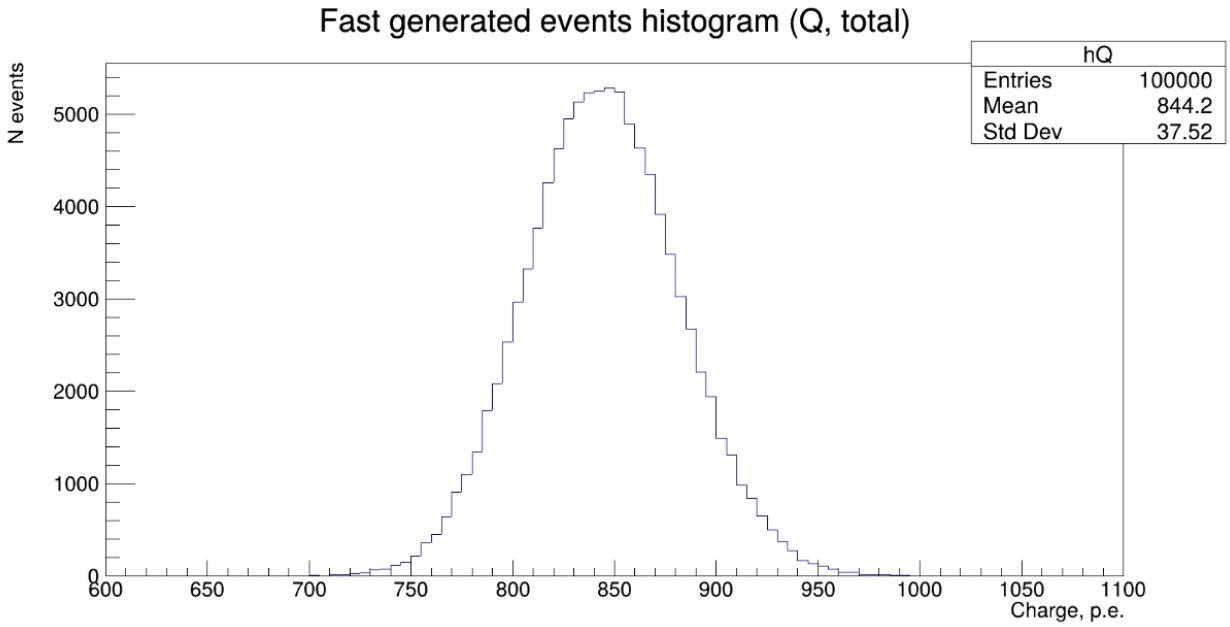

Figure 4.3 - Distribution of the total charge collected by PMTs of both types (Hamamatsu and NNVT) obtained from the fast simulation

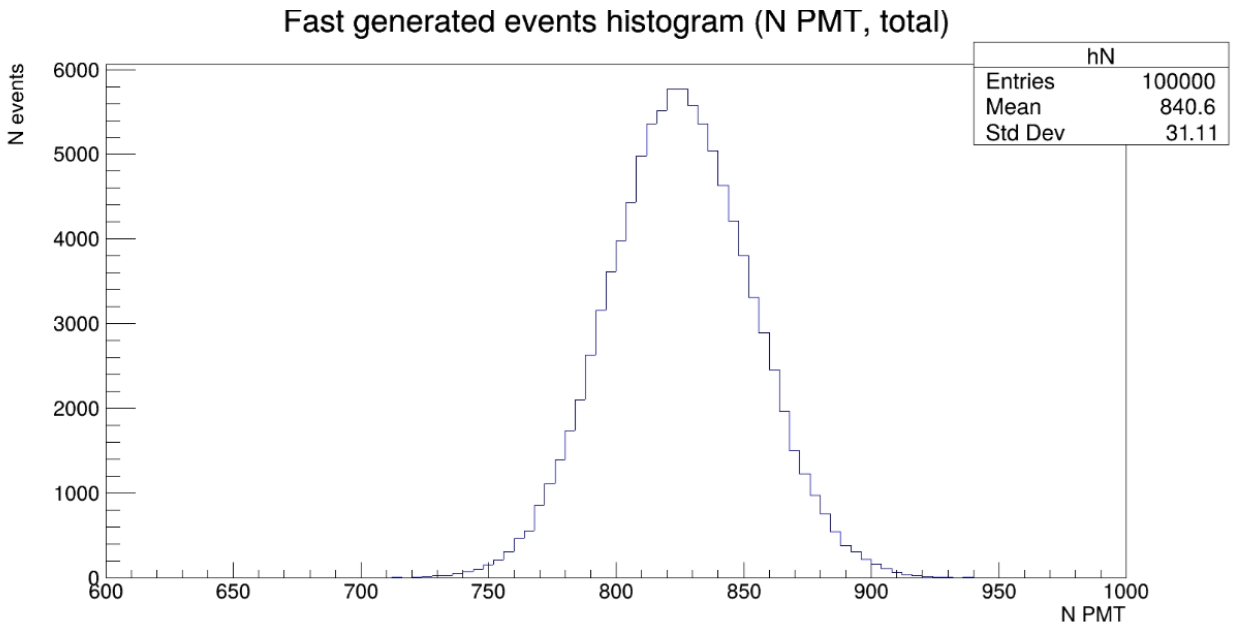

Figure 4.4 - Distribution of the number of fired PMTs of both types (Hamamatsu and NNVT) obtained from the fast simulation

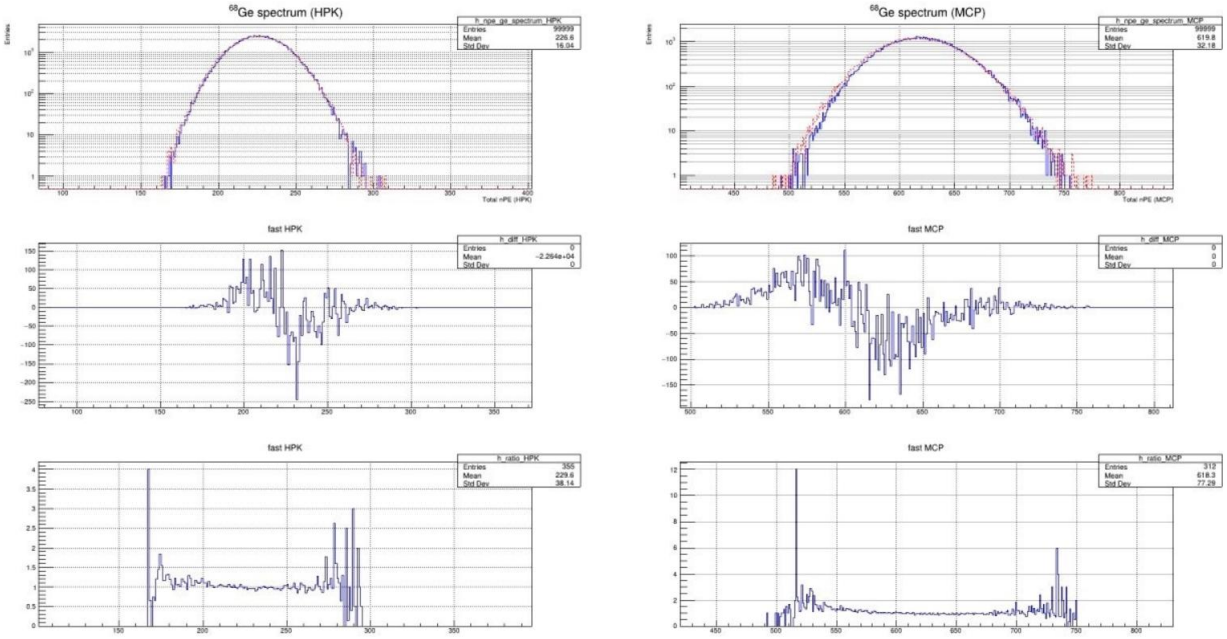

Figure 4.5 - Comparison of the fast (red) and slow (blue) simulations. Upper panels: charge distributions by PMT type; middle panels: difference (fast - slow); lower panels: ratio (slow / fast). Left column: Hamamatsu; right column: NNVT.

4.4. Energy resolution

To estimate the energy resolution, the histograms of the total collected charge and the number of fired PMTs were fitted with a Gaussian distribution. The table

shows the obtained values of the mean μ and sigma σ for the fast and slow simulations.

Simulation	Estimator	μ	σ	$R = \sigma/\mu$
Fast	Charge Q	844.2	37.52	$4.44\% \pm 0.01\%$
Fast	Number of PMTs N	840.6	31.11	$3.70\% \pm 0.01\%$
Slow	Charge Q	846.4	37.16	$4.39\% \pm 0.01\%$
Slow	Number of PMTs N	840.8	31.61	$3.76\% \pm 0.01\%$

The obtained χ^2/ndf values, close to 1–2.5, indicate good agreement between the fast and slow simulations. The slight excess of χ^2/ndf for MCP may be due to simplifications in the fast model (absence of signal time structure, absence of trigger window checking) or to statistical fluctuations in the slow simulation. The spread in sensitivities has almost no effect on the resolution.

The obtained resolution values (3.7–4.4%) are higher than the expected value for JUNO of $2.95\%/\sqrt{E}$ for electrons with an energy of 1 MeV. For a particle of ^{210}Po with an energy of 5.3 MeV, the expected resolution is ≈ 1.28%. The main reason for this discrepancy is the ionization quenching effect (Birks' quenching), which for heavy charged particles leads to a significant nonlinearity of the light yield.

Conclusion and outlook

In the course of this work, a fast simulation model of the JUNO detector response based on the slow simulation was developed and validated.

First, from the slow simulation of polonium-210 alpha decay at the center of the detector, the values of μ_0 - the average charge collected by a single PMT - were obtained. For the two types of photomultiplier tubes (Hamamatsu and NNVT), they were 0.04527 and 0.04904, respectively. These values were then passed to the developed fast event generator.

After that, a comparison between the fast and slow simulations was performed. For this purpose, a separate script was written that constructed histograms of charge distributions for each PMT type, calculated the differences and ratios, and computed the χ^2/ndf criterion. The obtained values were 1.62 for Hamamatsu and 2.55 for NNVT, indicating good agreement between the two approaches.

The energy resolution obtained from the fast simulation was about 4.4% for the total charge and about 3.7% for the number of fired PMTs. These values were almost identical to the results of the slow simulation, which confirms the correctness of the developed algorithm.

Thus, a fast model of the JUNO detector response has been successfully created and validated in this work. It can be used for further analysis of events within the detector volume and, in the future, for processing real data from the experiment.

Acknowledgements

I express my deep gratitude to my research supervisor Oleg Yuryevich Smirnov for setting the problem, explaining complex theoretical issues, and helping at all stages of this work.

I sincerely thank Kirill Klavdievich Kiselev for his willingness to answer my questions, explain the details of the simulation, and help with the difficulties that arose during the research.

I am also grateful to the entire team of the Joint Institute for Nuclear Research (JINR) for their warm welcome and for creating a comfortable working atmosphere.

I would like to specifically thank the START program for providing the opportunity to come to Dubna, for arranging my accommodation, and for the financial support throughout my participation.

References

1. Смирнов О. Habilitation thesis - Прямое измерение потока солнечных pp-нейтрино на детекторе Борексино. — URL: https://dissertations.jinr.ru/ru/Dissertations/Announcement/235.

2. JUNO collaboration. JUNO physics and detector // Progress in Particle and Nuclear Physics. — 2022. — Vol. 123. — P. 103927. — ISSN 0146-6410.

3. Determination of the neutrino mass hierarchy at an intermediate baseline / L. Zhan [et al.] // Phys. Rev. D. — 2008. — Vol. 78, issue 11. — P. 111103.

4. JUNO conceptual design report / Z. Djurcic [et al.]. — 2015.

5. Prediction of energy resolution in the JUNO experiment / A. Abusleme [et al.] // Chinese Physics C. — 2025. — Vol. 49, no. 1. — P. 013003.

6. Mass testing and characterization of 20-inch PMTs for JUNO / A. Abusleme [et al.] // The European Physical Journal C. — 2022. — Vol. 82, no. 12. — P. 1168. — ISSN 1434-6052.